Electronic Supplementary Material (ESI) for Journal of Materials Chemistry A.

Supplementary Information

Aqueous Manganese-Lead battery for large-scale energy storage

Jianhang Huang,[a,b] Lei Yan,[a] Duan Bin,[a] Xiaoli Dong,[a] Yonggang Wang*[a] and Yongyao Xia*[a,c]

a. Department of Chemistry and Shanghai Key Laboratory of Molecular Catalysis and Innovative Materials, Institute of New Energy, iChEM (Collaborative Innovation Center of Chemistry for Energy Materials), Fudan University, Shanghai 200433, China.

b. School of Materials Science and Engineering, Nanchang Hangkong University, Nanchang 330063, China.

c. Key Laboratory of the Ministry of Education for Advanced Catalysis Materials, Department of Chemistry, Zhejiang Normal University, Jinhua 321004, China.

Supplementary Figures

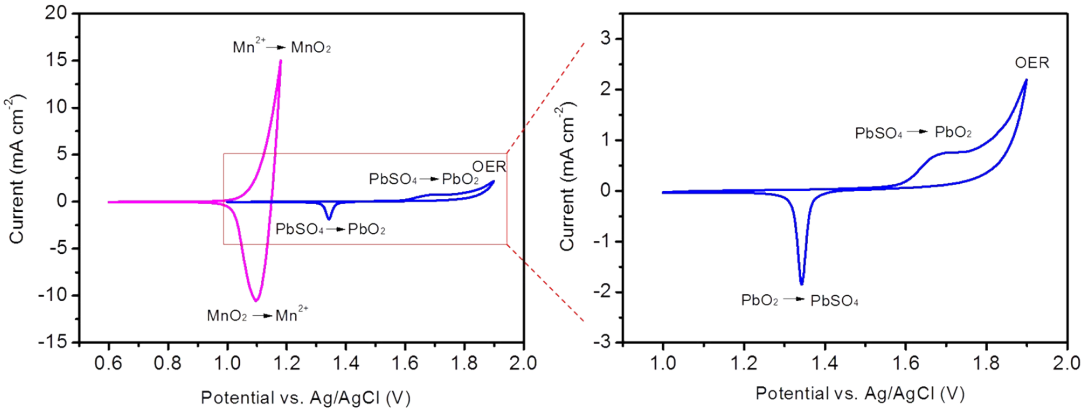

Figure S1. Comparison between cyclic voltammetry (CV) of Mn^{2+}/MnO_2 and $PbSO_4/PbO_2$. CV for 1 cm^2 carbon felt in the electrolyte containing 1 M $MnSO_4$ + 0.5 M H_2SO_4 at a sweep rate of 1 mV s^{-1} (pink curve) and 1 cm^2 PbO_2 electrode in the electrolyte containing 0.5 M H_2SO_4 at a sweep rate of 1 mV s^{-1} (blue curve). From the enlarged CV of 1 cm^2 PbO_2 electrode in the electrolyte containing 0.5 M H_2SO_4 at a sweep rate of 1 mV s^{-1}, it can be seen that the peak separation of Mn^{2+}/MnO_2 is much smaller than that of $PbSO_4/PbO_2$, and the response current density is much higher than that of $PbSO_4/PbO_2$, indicating the faster kinetics of Mn^{2+}/MnO_2 than $PbSO_4/PbO_2$.

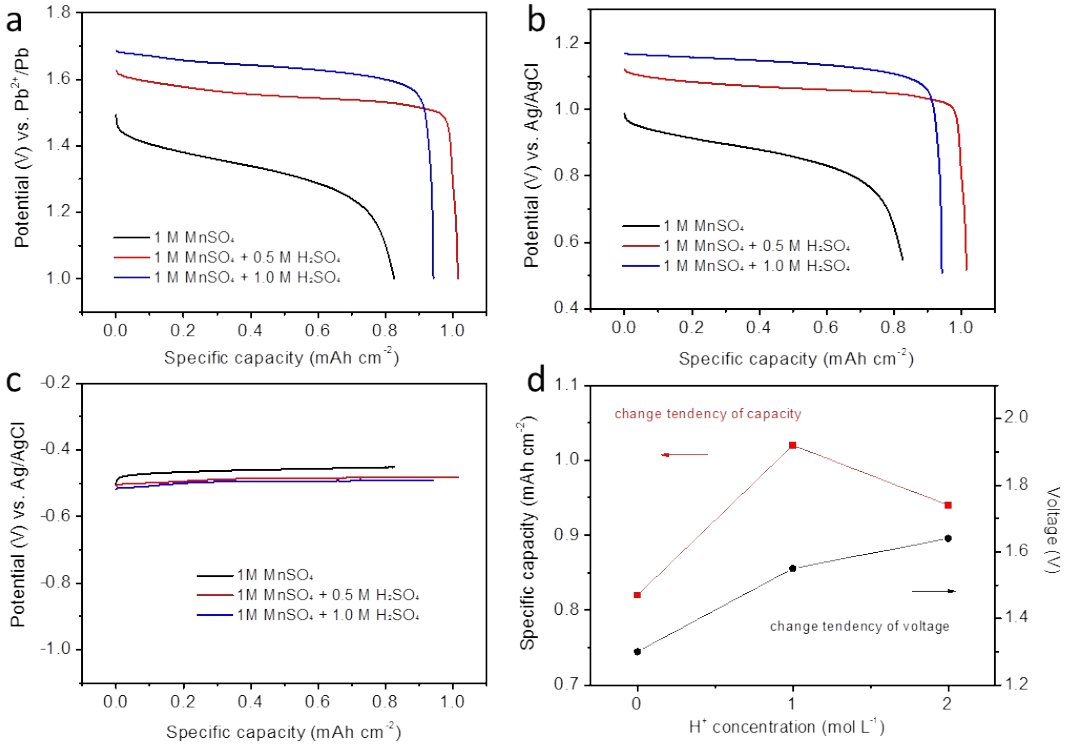

Figure S2. The influence of H^+ concentration on the discharge profiles of Mn-Pb battery. (a) The discharge profiles of Mn-Pb batteries using electrolyte with different acidity (0 M H_2SO_4, 0.5 M H_2SO_4 and 1 M H_2SO_4 respectively). The batteries are charged under 1.8 V to 1 mAh cm^{-2}, and then discharged at 10 mA cm^{-2} to 1 V. **(b,c)** The potential profiles (vs. Ag/AgCl) of cathodes **(b)** and anodes **(c)** using electrolyte with different acidity. **(d)** The variation tendency of capacity and voltage of batteries along with the electrolyte acidity.

The increase of discharge potential of the Mn-Pb battery can be explained by the Nernst equation:

$$Mn^{2+} + 2H_2O \leftrightarrow MnO_2 + 4H^+ + 2e^- \qquad (a)$$

$$\varphi = \varphi^{\theta} + \frac{RT}{nF} ln \frac{[a(H^+)]^4}{[a(Mn^{2+})]^1} \qquad (b)$$

where equation (a) is the overall redox reaction of MnO_2/Mn^{2+}, and equation (b) is the Nernst equation. φ is electrode potential, φ^{θ} is standard electrode potential, R is gas constant (8.314 J $K^{-1}mol^{-1}$), T is the temperature (298 K), F is faraday constant (96485 J $mol^{-1}V^{-1}$), n is the number of electron involved in reaction, a (species) is the concentration of species when the activity coefficients is 1. So from equation (b) we know that when the concentration of sulfuric acid increases, the potential for redox of MnO_2/Mn^{2+} will increase.

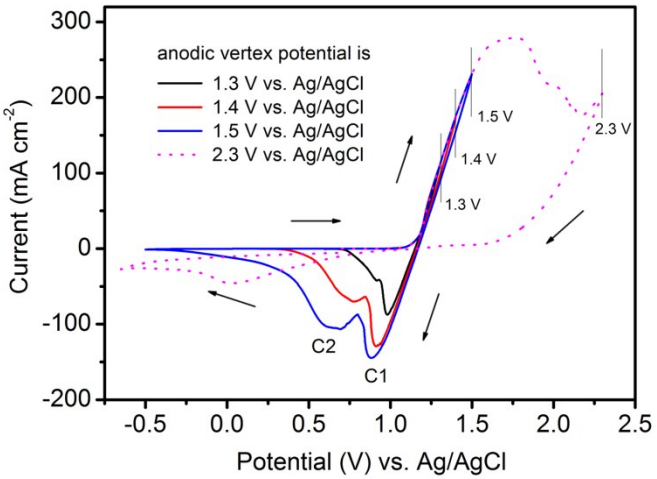

Figure S3. The evolution of cathodic peaks of MnO_2/Mn^{2+} with different anodic vertex potential. The CV curves of carbon felt in the electrolyte containing 1 M $MnSO_4$ and 0.5 M H_2SO_4 at a sweep rate of 1 mV s^{-1} with anodic vertex potential of 1.3 V to 1.5 V vs. Ag/AgCl, respectively. With the increase of anodic vertex potential, the area of C2 peak becomes large and roughly equivalent to the C1 peak. In addition, further increasing the vertex potential (pink dashed curve) will make the deposited MnO_2 irreversible, it is possibly because that the MnO_2 crystal formed under too high voltage is hard to be reduced.

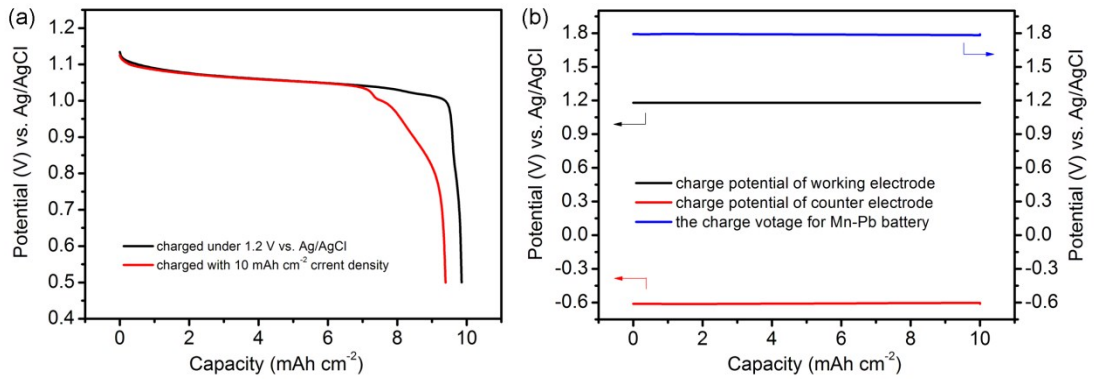

Figure S4. Comparison of discharge curves for the MnO_2 electrode with different charging technology and the determination of charge voltage of Mn-Pb battery. (a) Discharge curve of MnO_2 electrode with constant-voltage charging technology (black curve) and constant-current charging technology (red curve). For the constant-voltage charging, the working electrode (carbon felt) is charged under 1.18 V vs. Ag/AgCl to 10 mAh cm^{-2} (charge potential of 1.18 V will make sure that the main redox of MnO_2/Mn^{2+} will follow Pathway 1), and discharged at 10 mA cm^{-2} to 0.5 V vs. Ag/AgCl. For the constant-current charging, the working electrode (carbon felt) is charged at 10 mA cm^{-2} to 10 mAh cm^{-2}, and discharged at 10 mA cm^{-2} to 0.5 V vs. Ag/AgCl. Three-electrode system is used in this testing, and the electrolyte is 1 M $MnSO_4$ + 0.5 M H_2SO_4, the working electrode is carbon felt, counter electrode is excess $PbSO_4$ electrode, and the reference electrode is Ag/AgCl. It can be seen that the discharge curve of working electrode using constant-voltage charge technique shows one discharge platform, strongly demonstrate that Pathway 1 is the main mechanism for redox of MnO_2/Mn^{2+}. However, the discharge curve of working electrode using constant-current charge technique shows obvious two discharge voltage platform, indicating that the constant-current charge technique is unable to control redox mechanism of MnO_2/Mn^{2+}. (b) The charge voltage of Mn-Pb battery when the working electrode (carbon felt) is charged under 1.18 V vs. Ag/AgCl. The potential of counter electrode ($PbSO_4$) is about – 0.61 V vs. Ag/AgCl, so the voltage for Mn-Pb battery is about 1.79 V. For convenience, a charge voltage of 1.8 V is chosen to charge the Mn-Pb battery in subsequent experiments.

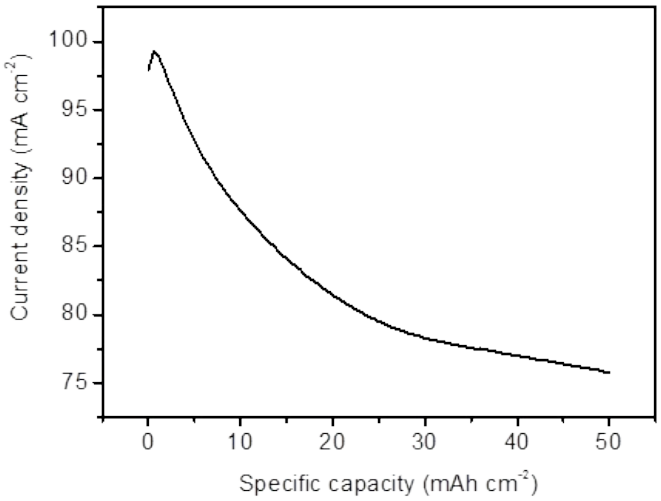

Figure S5. The charge current profile of Mn-Pb battery. The battery is charged under 1.8 V to 50 mAh cm^{-2}.

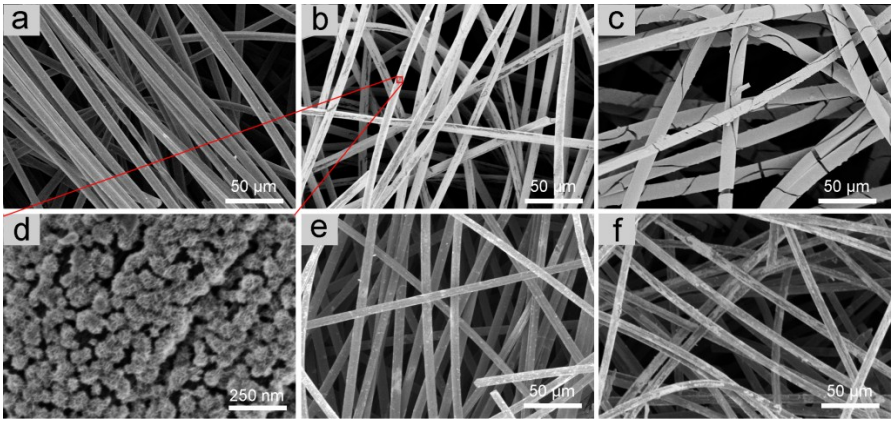

Figure S6. Morphology of carbon felt during the charge/discharge process. (a-c) The bare carbon felt **(a)**, carbon felt with 1 mAh cm^{-2} **(b)** and 50 mAh cm^{-2} **(c)** deposition capacity. **(d)** Enlarged view of the carbon felt with 1 mAh cm^{-2} deposition capacity. **(e,f)** The morphology after discharging to 1 V for the carbon felt with 1 mAh cm^{-2} **(e)** and 50 mAh cm^{-2} **(f)** deposition capacity. The batteries are charged under 1.8 V to 1 and 50 mAh cm^{-2} respectively and discharged at 10 mA cm^{-2} to 1 V.

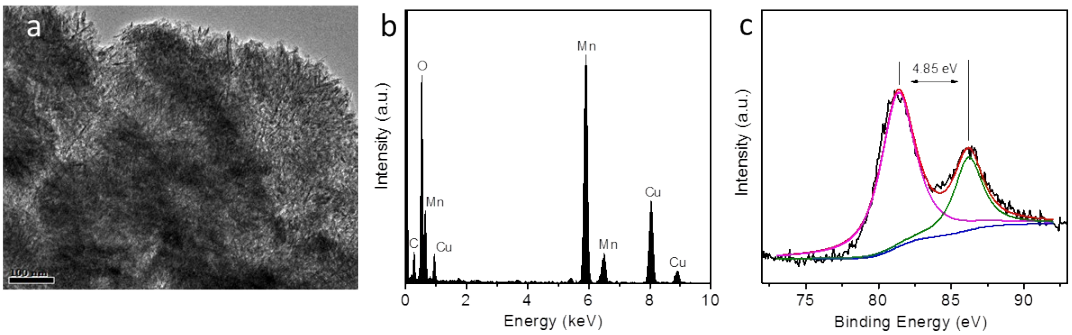

Figure S7. Characterization of the deposit on carbon felt during the charge process. (a) TEM image for the deposit on carbon felt with 10 mAh cm^{-2} deposition capaciry. **(b)** EDS analysis of the deposit on carbon felt. **(c)** XPS spectra of the deposit. The spin-energy separation of Mn 3s doublet is 4.85 eV, indicating that the deposit formed during charge process mainly containing MnO_2.

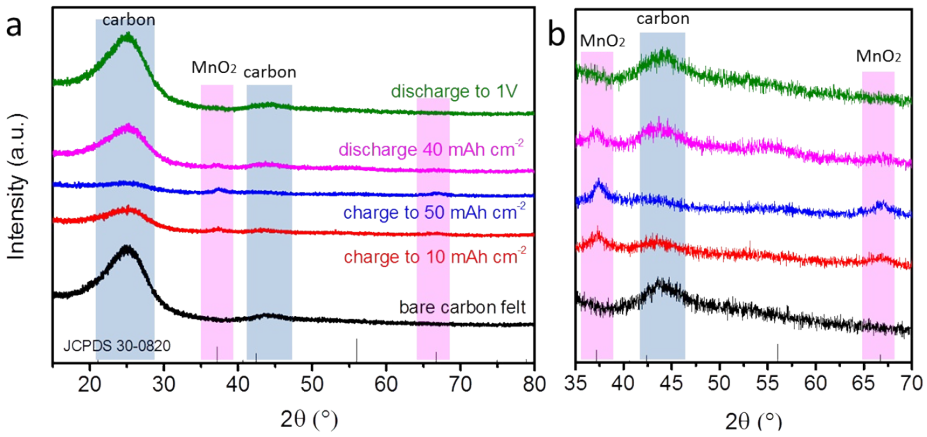

Figure S8. Evolution of XRD patterns during charge/discharge process. (a) With the deposition of MnO_2 (charging process), the carbon diffraction peaks at 26° and 44° shrink rapidly due to the shield of the deposited MnO_2 on the surface of carbon felt. And during the discharge process, the carbon diffraction peaks are recovered. **(b)** The enlarged view of **(a)** from 35° to 70°. With the shrink of carbon diffraction peak, new diffraction peaks at 37°and 67° emerge, which can be assigned to the (100), (102) and (110) planes of akhtenskite MnO_2 (JCPSD 30-0820).

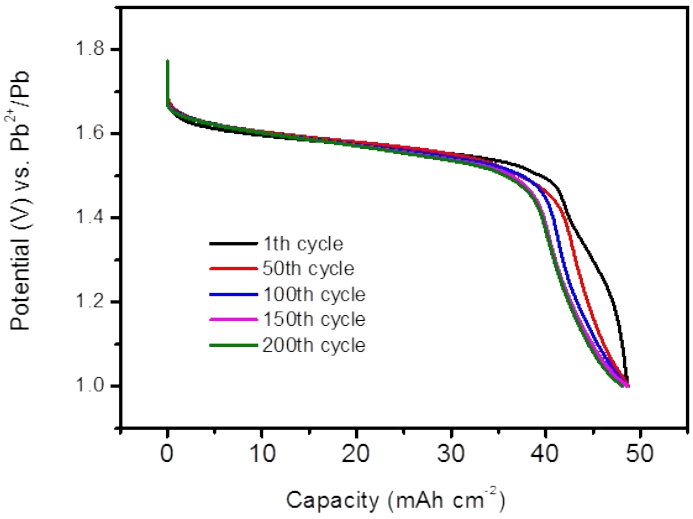

Figure S9. Evolution of discharge profiles for the battery with 50 mAh cm^{-2} deposition capacity. The battery is charged under 1.8 V to 50 mAh cm^{-2}, and then discharged at 10 mA cm^{-2} to 1 V.

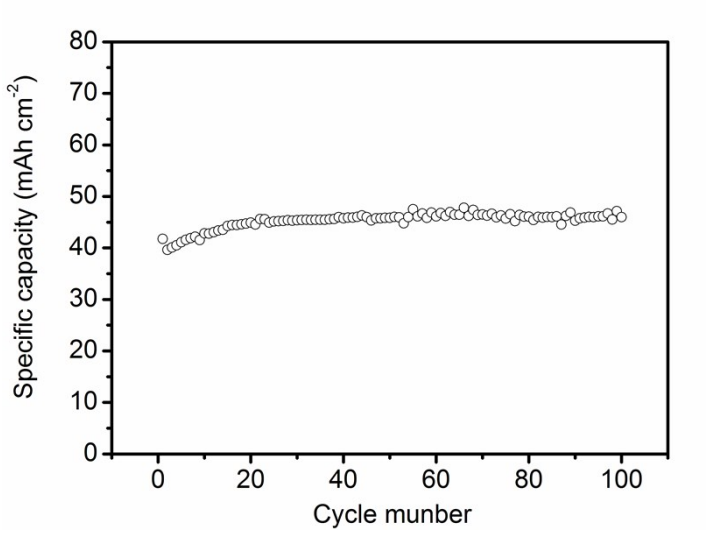

Figure S10. Cycle performance of Mn-Pn battery at high discharge current density of 40 mA cm^{-2}. The cell is charged under 1.8 V to 50 mAh cm^{-2} and discharged at 40 mA cm^{-2} to cut-off voltage of 1 V. It shows an average 45.3 mAh cm^{-2} with 90.6 % Coulombic efficiency over 100 cycles.

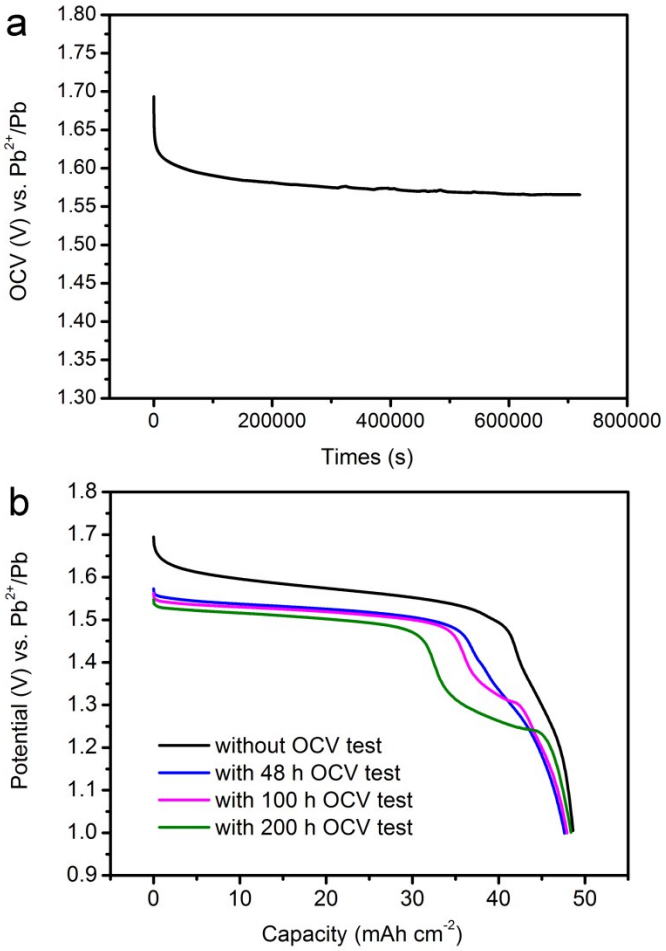

Figure S11. Self-discharge performance of the Mn-Pb battery. (**a**) Variation tendency of open circuit potential (OCV) during 200 hours settling time. The battery is charged under 1.8 V to 50 mAh cm^{-2} first. (**b**) The comparison of discharge curves (discharged current is 10 mA cm^{-2} to 1 V) for the battery with 0 (black curve), 48 (blue curve), 100 (violet curve) and 200 hours (green curve) OCV test.

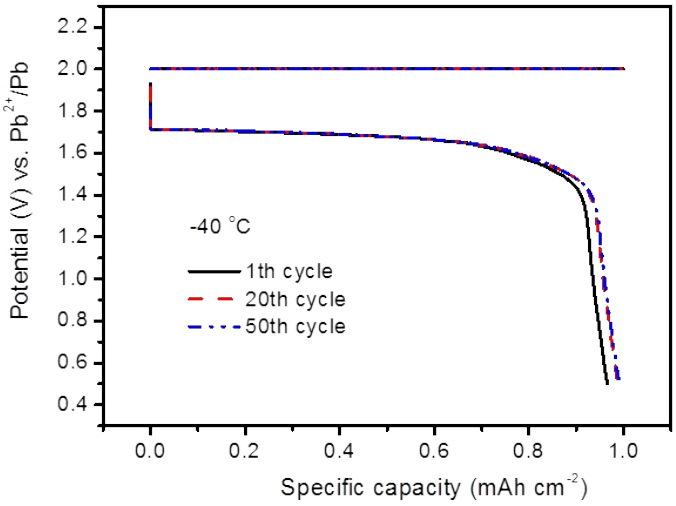

Figure S12. Charge/discharge profiles of Mn-Pb battery at -40 °C . 3 M H_2SO_4 +1 M H_2SO_4 is used as electrolyte in order to decrease the freezing point, the battery is charged under 2V and discharged at 0.2 mA cm^{-2}. Both charge and discharge process are conducted at -40 °C .

Figure S13. Exhibition of the components for the pouch battery. The pouch battery consists of one piece of carbon felt (40 × 50 × 5 mm) as cathode current collector, one piece of $PbSO_4$ anode (40 × 50 mm) and a filter paper is used as separator.

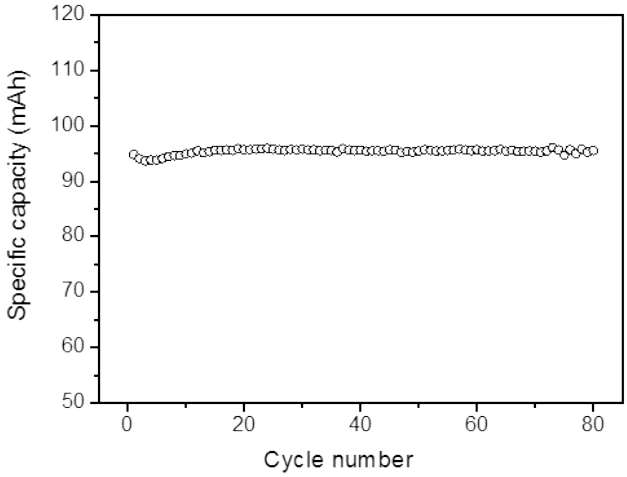

Figure S14. Cycle performance of pouch battery. The battery is charged under 1.8 V to 100 mAh, and discharged at 50 mA to 1 V.

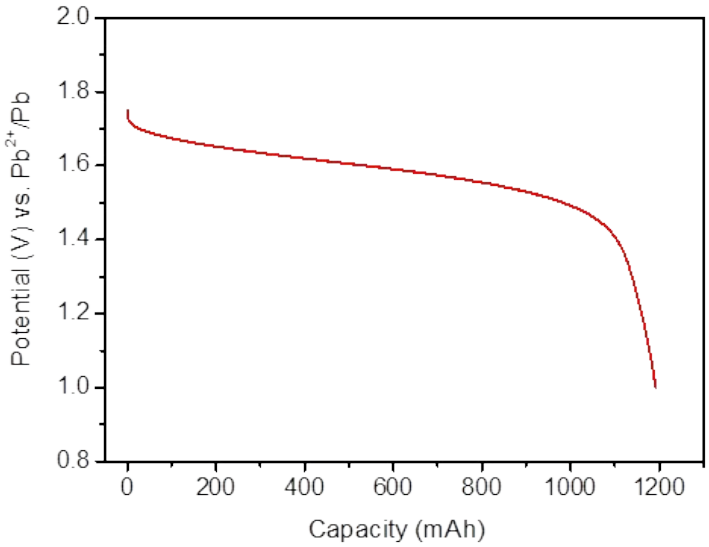

Figure S15. Capacity determination of the Mn-Pb pouch battery using 10 mL electrolyte with 3 M $MnSO_4$ and 0.5 M H_2SO_4. The battery is charged under 1.8 V to theoretical capacity of 1608 mAh, and discharged at 20 mA to 1 V. The actual discharge capacity and energy is 1192 mAh and 1.87 Wh, respectively, corresponding to a high volumetric energy density of 187 Wh L^{-1} based on volume of electrolyte, and 124.6 Wh L^{-1} at the battery level (the volume of entire battery is about 15 cm^3). The active material for positive redox chemistry is $MnSO_4$ in electrolyte, which is 4.53 g. And the anode material is $PbSO_4$, which is 12 g. So based on the actual mass of the cathode and anode materials, the gravimetric energy density of Mn-Pb pouch battery is 113 Wh kg^{-1}.

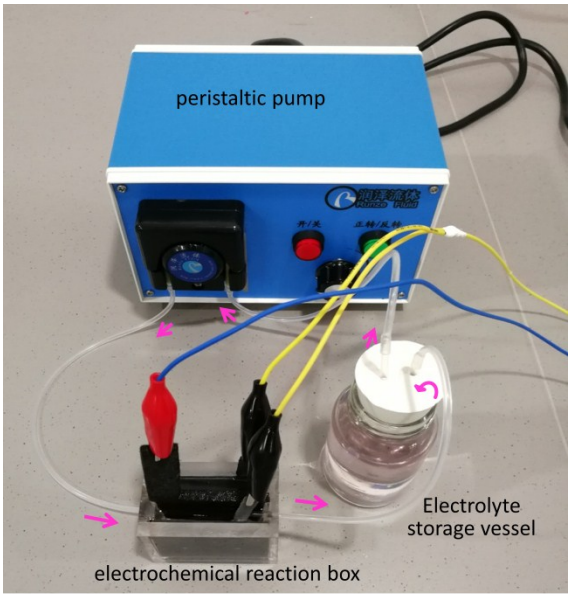

Figure S16. Exhibition of the flow-assisted Mn-Pb battery. Photograph of the assembled flow-assisted Mn-Pb battery. The pink arrows show the flow direction of electrolyte.

Supplementary Tables

Cost estimation

The main cost of the Mn-Pb cell is $MnSO_4 \cdot H_2O$, H_2SO_4 and Pb. And the average price of $MnSO_4 \cdot H_2O$ (electroplating grade) is US$ 0.55 kg^{-1}, 98% H_2SO_4 is US$ 0.2 kg^{-1}, and Pb is US$ 2.15 kg^{-1}, which was obtained from www.alibaba.com. The cost of the cell is calculated according to the following equation: $P = \sum_i p_i m_i / E$, where P is the capital cost per unit of discharged electrical energy (US$ kWh^{-1}), p_i is the cost per unit of above materials used in Mn-Pb cell (US$ kg^{-1}), m_i is the mass of materials (kg), and E is the discharged energy of the cell (kWh), which is obtained from the pouch Mn-Pb battery. And the detailed calculation is presented in Supplementary **Table S1**.

Table S1. Capital cost estimation of a pouch battery. The pouch battery contains 10 mL 0.5 M H_2SO_4 + 3 M $MnSO_4$ electrolyte, Pb anode and carbon felt as cathode current collector

	H_2SO_4	$MnSO_4 \bullet H_2O$	Pb	total
n_i / mol	0.005	0.03	0.03	
M_i / g mol^{-1}	100 (98%)	169	207	
m_i / g	0.5	5.07	6.21	
p_i / US$ kg^{-1}	0.2	0.55	2.15	
$p_i m_i$ / US$	0.0001	0.0028	0.013	0.016
E / Wh	1.87			
P / US$ kWh^{-1}	**8.6**			
F / C mol^{-1}	96485.4			

Table S2. Cost comparisons of the Mn-Pb battery to the current state-of-the-art battery systems for large-scale energy storage

Technology option	Maturity	Cost (US$ kWh^{-1})	Reference
Li-Sb-Pb liquid metal battery	research	65 based on electrode materials	1
AQDS-Br_2 flow[a]	research	27 based on electrolyte	2
Zn-ion battery	research	60 based on electrode materials	3
Li-ion battery	commercial	250-2000	4-9
Na-S	commercial	450-550	5, 8
Zn-Br flow	demo	300-350	6, 8
V redox	demo	400-1500	5, 8
Pb-acid	commercial	50-500	5, 8, 10
Mn-Pb battery	**research**	**8.6 based on electrolyte and electrode**	**Our work**

[a] AQDS = 9,10-anthraquinone-2,7-disulphonic acid

All the references in supplementary information are also cited in main-text.

Table S3. Performance comparisons of the Mn-Pb battery to the current state-of-the-art battery systems for large-scale energy storage

Technology option	No. of Cycles	Energy density	Reference
Li-Sb-Pb liquid metal battery	450 (94% retention)	-	1
AQDS-Br_2 flow[a]	15 (without decay)	50 Wh L^{-1} based on electrolyte	2
TEMPO-viologen flow[b]	10000 (80% retention)	10 Wh L^{-1} based on electrolyte	11
K-ion battery	2000 (73% retention)	80 Wh kg^{-1} based on cathode and anode	12
Li-ion*	2000	300 Wh kg^{-1}	8, 13, 14
Na-S*	4000	200 Wh kg^{-1}	8, 15
Zn-Br flow	10000	70 Wh kg^{-1}	8, 16, 17
V redox	10000	40 Wh L^{-1}	8, 18
Pb-acid	< 1000 cycle	50 Wh kg^{-1}	8, 10, 15
Mn-Pb battery	**10000 (without decay)**	**187 Wh L^{-1} based on electrolyte, 113 Wh kg^{-1} based on cathode and anode**	**Our work**

[a] AQDS = 9,10-anthraquinone-2,7-disulphonic acid

[b] TEMPO = 2,2,6,6-tetramethylpiperidinyloxyl, viologen = 4,4 9-bipyridine derivative

* Li-ion and Na-S battery possess high energy density. However, the safety issue (such as flammability and explosion of Li-ion battery, thermal runaway of Na-S battery that must work under high temperature) is a great challenge for the large-scale energy storage. Whereas, the Mn-Pb battery shows high safety, low cost and long cycle life, which are more important to the large-scale energy storage.

All the references in supplementary information are also cited in main-text.

Supplementary Video

Video S1: Exhibition of the pouch Mn-Pb battery.

The toy car works smoothly when powered by two pouch battery in series connection (the toy car requires a power ~ 2 W).

Video S2: Penetration test of the Mn-Pb battery.

A mini-fan (requiring a power of ~ 500 mW) can be powered by one pouch battery. Although the rotational speed of the mini-fan is lowered by the nail penetration, it can be recovered immediately after remove of nails, which shows high tolerance against battery abuse.

Supplementary Reference (All the references in supplementary information are also cited in main-text)

1. K. Wang, K. Jiang, B. Chung, T. Ouchi, P. J. Burke, D. A. Boysen, D. J. Bradwell, H. Kim, U. Muecke and D. R. Sadoway, *Nature*, 2014, **514**, 348-350.
2. B. Huskinson, M. P. Marshak, C. Suh, S. Er, M. R. Gerhardt, C. J. Galvin, X. Chen, A. Aspuru-Guzik, R. G. Gordon and M. J. Aziz, *Nature*, 2014, **505**, 195-198.
3. D. Kundu, B. D. Adams, V. Duffort, S. H. Vajargah and L. F. Nazar, *Nat. Energy*, 2016, **1**, 16119.
4. B. Dunn, H. Kamath and J. M. Tarascon, *Science*, 2011, **334**, 928-935.
5. O. Schmidt, A. Hawkes, A. Gambhir and I. Staffell, *Nat. Energy*, 2017, **2**, 17110.
6. R. M. Darling, K. G. Gallagher, J. A. Kowalski, S. Ha and F. R. Brushett, *Energy Environ. Sci.*, 2014, **7**, 3459-3477.
7. Z. P. Cano, D. Banham, S. Ye, A. Hintennach, J. Lu, M. Fowler and Z. Chen, *Nat. Energy*, 2018, **3**, 279-289.
8. B. Zakeri and S. Syri, *Renew. Sust. Energy Rev.*, 2015, **42**, 569-596.
9. B. Nykvist and M. Nilsson, *Nat. Clim. Chang.*, 2015, **5**, 329-332.
10. J. O. G. Posada, A. J. R. Rennie, S. P. Villar, V. L. Martins, J. Marinaccio, A. Barnes, C. F. Glover, D. A. Worsley and P. J. Hall, *Renew. Sust. Energy Rev.*, 2017, **68**, 1174-1182.
11. T. Janoschka, N. Martin, U. Martin, C. Friebe, S. Morgenstern, H. Hiller, M. D. Hager and U. S. Schubert, *Nature*, 2015, **527**, 78-81.
12. L. Jiang, Y. Lu, C. Zhao, L. Liu, J. Zhang, Q. Zhang, X. Shen, J. Zhao, X. Yu, H. Li, X. Huang, L. Chen and Y.-S. Hu, *Nat. Energy*, 2019, **4**, 495-503.
13. J. Liu, Z. Bao, Y. Cui, E. J. Dufek, J. B. Goodenough, P. Khalifah, Q. Li, B. Y. Liaw, P. Liu, A. Manthiram, Y. S. Meng, V. R. Subramanian, M. F. Toney, V. V. Viswanathan, M. S. Whittingham, J. Xiao, W. Xu, J. Yang, X.-Q. Yang and J.-G. Zhang, *Nat. Energy*, 2019, **4**, 180-186.
14. R. Schmuch, R. Wagner, G. Hörpel, T. Placke and M. Winter, *Nat. Energy*, 2018, **3**, 267-278.
15. Z. Yang, J. Zhang, M. C. Kintner-Meyer, X. Lu, D. Choi, J. P. Lemmon and J. Liu, *Chem. rev.*, 2011, **111**, 3577-3613.
16. M. Skyllas-Kazacos, M. H. Chakrabarti, S. A. Hajimolana, F. S. Mjalli and M. Saleem, *J. Electrochem. Soc.*, 2011, **158**, R55.
17. T. M. Gur, *Energy Environ. Sci.*, 2018, **11**, 2696-2767.
18. J. Winsberg, T. Hagemann, T. Janoschka, M. D. Hager and U. S. Schubert, *Angew. Chem. Int. Edit.*, 2017, **56**, 686-711.